Layer-by-Layer Fabrication of High-Performance Broadband Anti-reflection Coatings Comprising Oppositely Charged Nanosheets and Nanoparticles

Xin Wu, Jinjuan Xue, Yuming Zhou, Shuaishuai Ma & Man He

School of Chemistry and Chemical Engineering, Southeast University,
Jiangsu Nanjing 211189, China
Email: xindaisy9063@hotmail.com

Abstract. In this study, we fabricated broadband anti-reflection coatings using a method based on layer-by-layer self assembly of positively charged layer double hydroxide (LDH) nanosheets and negatively charged silica nanoparticles via electrostatic interaction. Scanning electron microscopy and atomic force microscopy were used to observe the morphology, structure, and surface topography of LDH/SiO_2 multilayer coatings. The anti-reflection properties of the coatings were investigated by UV visible spectrophotometry. Glass substrates covered with the LDH/SiO_2 multilayer coatings exhibited broadband anti-reflection properties. The obtained $[LDH(0.4\ g/L)/SiO_2(25\ nm)]_8$, $[LDH(0.4\ g/L)/SiO_2(50\ nm)]_{10}$, and $[LDH(0.8\ g/L)/SiO_2(25\ nm)]_6$ coatings exhibited the best broadband anti-reflection properties among the as-prepared LDH/SiO_2 multilayer coatings with different deposition cycles. Transmission levels of 97% were achieved in these optimal systems. Moreover, a maximum transmittance of 98% was achieved at a wavelength of 550 nm in the $[LDH(0.4\ g/L)/SiO_2(25nm)]_8$ system and at 700 nm in the $[LDH(0.8\ g/L)/SiO_2(25nm)]_6$ system. Different packing patterns of the two oppositely charged nanomaterials (dense packing of LDH nanosheets and loose stacking of silica nanoparticles) and the moderate textured surface of the coatings contributed to the enhanced light transmission and reduced wavelength dependence in the UV visible spectral range.

Keywords: *anti-reflection; layer-by-layer; broadband; LDH nanosheets; silica nanoparticles.*

1 Introduction

Anti-reflection (AR) coatings can effectively reduce reflective losses at interfaces to enhance the transmittance of light. Therefore, they have important applications in photovoltaic and displaying devices and all kinds of optical lenses [1-3]. According to the AR requirement [4], for a glass substrate ($n_s = 1.5$), the refractive index (n) of AR material should be 1.22 to meet complete zero reflectance at a specific wavelength [5,6]. However, natural materials with such a low refractive index are either rare or expensive to obtain

Received May 2nd, 2015, Revised July 26th, 2015, Accepted for publication September, 9th, 2015
 ISSN: 2337-5779, DOI: 10.5614/j.eng.technol.sci.2015.47.5.5

in thin film form. One approach to lower the refractive index is to design a nanoporous structure of the AR coatings, since the introduction of nanopores can reduce the refractive index of the coatings and satisfy the AR requirement [7,8]. Such nanoporous materials can possess a low effective refractive index due to the introduction of air, which has the lowest possible refractive index of 1.00 [4].

The layer-by-layer (LbL) technique is an attractive method for preparation of antireflection materials because it can produce large-area, uniform, and defect-free nanoporous coatings on essentially any type of surface, with precise control over the thickness and optical properties [9-11]. For example, Zhang, *et al*. reported a method for the fabrication of mechanically stable antireflection and antifogging silica coatings by LbL deposition of poly dimethyl diallyl ammonium chloride (PDDA)/silicate complexes with polyacrylic acid (PAA) on quartz substrates followed by calcination [8]. Shimomura, *et al*. reported 4-stack high-performance broadband antireflection coatings with the materials of SiO_2, ammonium perchlorate SiO_2($APSiO_2$), TiO_2 and phenyl vinyl group (PVS) by LbL technique [12]. Zhang, *et al*. developed a rapid and substrate-independent LbL assembly method for the fabrication of AR and antifogging-integrated coatings by three deposition cycles of SiO_2/PDDA coatings [13]. However, to our knowledge, few papers have reported on the fabrication of broadband AR multilayer films containing oppositely charged nanoparticles/ nanosheets by the LbL technique.

In this study, we fabricated anti-reflection coatings based on layer-by-layer self-assembly of positively charged LDH nanosheets and negatively charged silica nanoparticles via electrostatic attraction. The LDH/SiO_2 multilayer coatings showed high-performance broadband anti-reflection properties. Among the three systems, namely [LDH(0.4 g/L)/SiO_2(25 nm)]$_n$, [LDH(0.4 g/L)/ SiO_2(50 nm)]$_n$, [LDH(0.8 g/L)/SiO_2(25 nm)]$_n$ (n = 2, 4, 6, 8, and 10), the maximum transmittance of 98% was achieved at a wavelength of 700 nm in the [LDH(0.8 g/L)/SiO_2(25 nm)]$_6$ system. In addition, transmission levels of 97% were achieved in the three systems, whereas the transmission level of the uncoated slide glass was only around 92% in the spectral range of 300 nm to 800 nm. Zhang [8] achieved a maximum transmittance of 99.86% in the visible spectral range for calcined PAA/PDDA-silicate films deposited on quartz substrates. Moreover, Zhang [13] achieved a maximum transmittance of 99.9% in the visible spectral range for ($MSiO_2$/PDDA)*3 coatings deposited on quartz substrates. The different materials added into the coatings maybe responsible for the lower transmittances. No polyelectrolytes were used in our coatings. LDHs are easier to prepare and cheaper than polyelectrolytes. We fabricated broadband anti-reflection coatings consisting of oppositely charged nanosheets/nanoparticles without using polyelectrolytes. The effect of the

morphology and structure of the coatings and the surface topography on the optical properties are discussed in detail below.

2 Materials and Experiments

2.1 Materials

Tetraethyl orthosilicate (TEOS, 99%) was purchased from Aldrich. $NH_3 \cdot H_2O$ (25%), EtOH (99.5%), Na_2CO_3, NaCl, NaOH, CH_3COONa, $Mg(NO_3)_2 \cdot 6H_2O$, $Al(NO_3)_3 \cdot 9H_2O$ were obtained from Sinopharm Chemical Regent Co. Ltd. Microscope glass slides (made in the USA from Swiss glass) used for the deposition were obtained from Aldrich. Water purified in a Milli-Q system was used during all the experiments.

2.2 Preparation of the LDH nanosheets

We combined the methods Hibino, *et al*. [14], Liu, *et al*. [15], and Iyi, *et al*. [16] have used before and set up the steps as follows:

(1) Synthesis of $CO_3 \cdot$ Mg-Al LDH. 0.01875 mol $Mg(NO_3)_2 \cdot 6H_2O$ and 0.00625 mol $Al(NO_3)_3 \cdot 9H_2O$ were dissolved in 50 mL of deionized water. An alkaline carbonate solution (1 M NaOH and 0.125 M Na_2CO_3) was added dropwise to the above solution under vigorous agitation until the pH of the reaction solution reached 10.5. Then the suspension was left standing in a water bath of 75 °C for 24 h. After filtration, the precipitate was washed repeatedly with deionized water, and dried at 60 °C for 12 h, thus yielding a white solid.

(2) Decarbonation and anion exchange of Mg-Al LDH. 1 g $CO_3 \cdot$ Mg-Al LDH was dispersed into 1 L acid-salt mixed solution (3.3 mMHCl and 1 M NaCl). After purging with nitrogen gas, the mixture was stirred at room temperature for 24 h, the resultant product was filtered and washed with deionized water and then dried in a vacuum to obtain Cl· Mg-Al LDH. 0.2 g as-prepared Cl· Mg-Al LDH was added to 100 ml of water solution containing 2.5 M CH_3COONa, the mixture was stirred vigorously at 35 °C for 24 h after purging with nitrogen gas and ultrasonification. The resulting suspension was filtered through a membrane filter with a pore size of 0.2 μm and thoroughly washed with degassed deionized water under nitrogen atmosphere. The remaining precipitates were collected on a filter and immediately dried in a vacuum to yield AcO· Mg-Al LDH.

(3) Exfoliation of Mg-Al LDH. 0.25 g AcO· Mg-Al LDH was dispersed in 625 mL decarbonated water; the concentration of the suspension was about 0.4 g/L. Then, the mixture was successively sonicated in an ultrasonic water bath

periodically for 30 min each time, until the turbidity of the dispersion remained constant. Water was the only solvent used throughout the procedure.

2.3 Preparation of the Silica Nanoparticles

Silica nanoparticles with diameters of approximately 25 and 50 nm were synthesized by Stöber method. Typically, $NH_3 \cdot H_2O$ and EtOH were added into a 250-mL three-neck flask and stirred for 10 min. Then, TEOS was added into the mixture and stirred at 50 °C for 12 h. The final molar ratio of TEOS:H_2O:EtOH:NH_3 was 1:(3.25 -6.31):37.6:(0.17 -0.34). Figure 1 shows the image of prepared silica sol. The silica nanoparticles were then dispersed in EtOH to reach a concentration of 0.5 wt%.

Figure 1 Silica sol prepared by Stöber method.

2.4 AR Coatings LbL Assembly

Microscope glass slides were cleaned by treatment in a bath of methanol/HCl (1:1 by volume) and then concentrated H_2SO_4 for 30 min each. The cleaned substrates were dipped into the LDH nanosheet suspension (0.4 or 0.8 g/L) for 15 min, followed by one 2-min and two 1-min rinsing steps by using deionized water. Then, the substrates were dipped into the aggregated nanoparticle solution for another 15 min, and rinsed in the same manner. The LbL procedure is shown in Figure 2. The alternating deposition procedures were performed for a proper number of cycles to obtain $(LDH/SiO_2)_n$ (n = 2, 4, 6, 8, and 10) coatings.

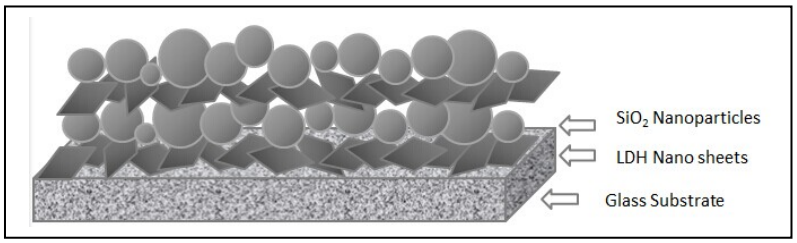

Figure 2 The LbL procedure of AR coatings.

2.5 Characterization

For the part of LDH materials characterization, X-ray diffraction (XRD) data were recorded with a Rigaku Rint-2000 diffractometer. The morphology of the exfoliated Mg-Al LDH nanosheets was examined with a Hitachi H-600 transmission electron microscope (TEM). For the AR coatings characterization, tapping mode atomic force microscopic (AFM) images were acquired under ambient conditions using an Agilent 5500 AFM/SPM system to demonstrate the surface topography. The surface and cross-sectional morphologies of the AR coatings were recorded using a Philips XL30 electron microscope (SEM) with an accelerating voltage of 20 kV.

3 Result and Discussion

Broadband anti-reflection coatings were successfully fabricated via layer-by-layer assembly of positively charged LDH nanosheets and negatively charged silica nanoparticles on glass substrates, thus yielding LDH/SiO_2 multilayer films. The self-assembly process is driven by electrostatic interaction between the oppositely charged nanomaterials.

The XRD pattern of the starting LDH material CO_3· Mg-Al LDH exhibited the characteristic basal reflections of LDH materials with sharp peaks of (003) and (006) at low 2θ angle, as well as weaker and less defined peaks at higher angular values [Figure 3(a)]. All diffraction peaks could be indexed as a rhombohedral structure (LDH) [15]. As shown in Figure 4(a), a transparent colloidal suspension was obtained after treating the as-prepared AcO· MgAl LDH with water, suggesting the occurrence of delamination. Clear Tyndall light scattering was observed for the suspension by a side-incident light beam, indicating the presence of exfoliated Mg-Al LDH nanosheet dispersed in water. The exfoliated MgAl LDH nanosheets suspension was well-dispersed and stable without any precipitation when stored in an N_2 atmosphere for a few weeks. By centrifugation at 12,000 rpm for 30 min, white glue-like aggregates were recovered from the suspension. The XRD pattern of the wet aggregates is

shown in Figure 3(b). The sharp basal reflections of LDH materials disappeared in this pattern, suggesting that the layer structure was collapsed. The appearance of amorphous-like halos at low 2θ angle can be attributed to the randomly aggregated nanosheets and the scattering of the glass substrate [17,18].

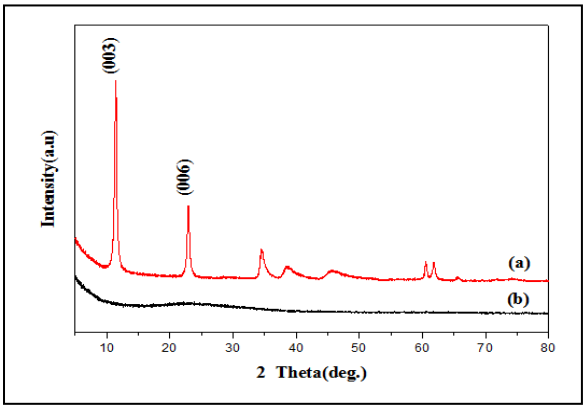

Figure 3 XRD patterns of (a) the starting LDH material CO_3· Mg-Al LDH and (b) glue-like aggregates centrifuged from the transparent suspension.

From a typical TEM image (Figure 4(b)), we observed that the thin sheet-like objects (tens of nanometers in lateral sizes) were morphologically irregular and dimensionally diminished, showing faint but homogeneous contrast, which indicated the breakage or fracture of sheets during the delimination process and reflected their ultrathin nature and uniform thickness [19].

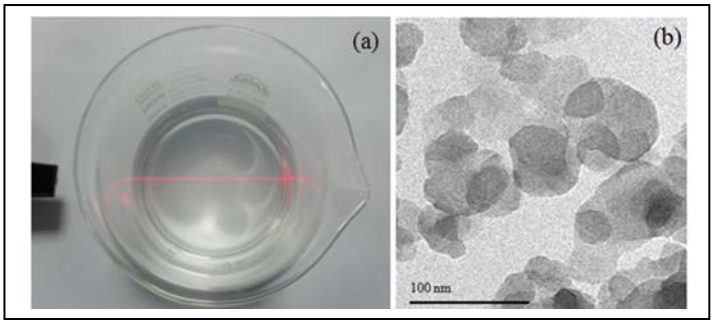

Figure 4 (a) Photograph of a colloidal suspension of exfoliated Mg-Al LDH nanosheets. The light beam was incident from the side to demonstrate the Tyndall effect. The LDH content was 0.4 g/L. (b) TEM image of Mg-Al LDH nanosheets.

Figure 5 shows top-view SEM images of $(LDH/SiO2)_6$ (the LDH content was 0.4 g/L or 0.8 g/L, and the diameter of silica nanoparticles was 25 or 50 nm)

coatings deposited on glass substrates. Top layers of coatings containing irregularly shaped aggregated silica nanoparticles with loose stacking pattern were observed. Different sizes of silica nanoparticles could clearly be distinguished. Nanopores were formed by the random packing of aggregated nanoparticles.

Moreover, the porous structure is beneficial to the anti-reflection property. From the cross-sectional SEM images in Figure 6, we can see the lack of uniform and linear surface boundaries on top of the coatings, which resulted from the hill-to-valley surfaces of the coatings created by the aggregated nanoparticles. Hence, the thickness of the coatings is difficult to measure accurately.

However, we clearly observed that the thickness of the coatings increased with the increasing number of LDH/SiO2 deposition cycles, indicating the success of layer-by-layer fabrication. The interface boundaries of the oppositely charged LDH nanosheets and silica nanoparticles were not obvious. In general, for MgAl LDH nanosheets exfoliated in water, large sheets show an average thickness of about 2.5 nm, whereas small sheets show thicknesses ranging between 0.55 nm to 0.95 nm, as has been noted by Hibino, *et al*. in [15].

The LDH nanosheet layers were extremely thin within the coatings, such that they were difficult to find easily in the cross-sectional SEM images. The small thickness dimension and sheet-like shape led us to reasonably suppose that LDH nanosheets can generate a dense packing pattern in the coatings during the LbL process. The loose stacking of silica nanoparticles and dense packing of LDH nanosheets are considered to result in different volume fractions in alternating layers, which causes discontinuous refraction index changes between the layers and creates a refractive index profile. The coatings fabricated by the abovementioned packing arrangement effectively suppresses reflection and reduces wavelength dependence in the UV-vis spectral range [20-22].

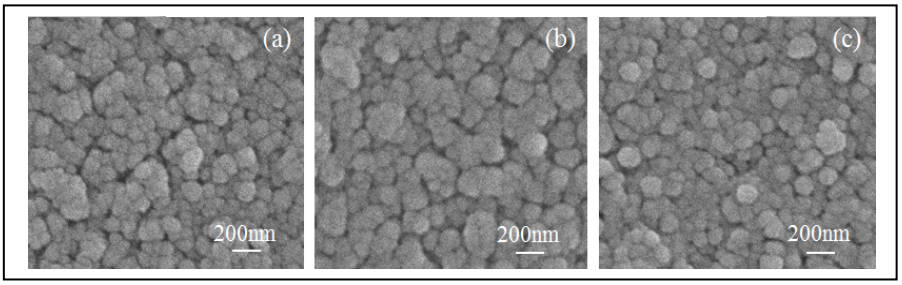

Figure 5 Top-view SEM images of (a) [LDH(0.4 g/L)/SiO_2(25 nm)]$_6$ (b) [LDH (0.4 g/L)/SiO_2(50 nm)]$_6$ and (c) [LDH(0.8 g/L)/SiO_2(25 nm)]$_6$ coatings deposited on the glass substrates.

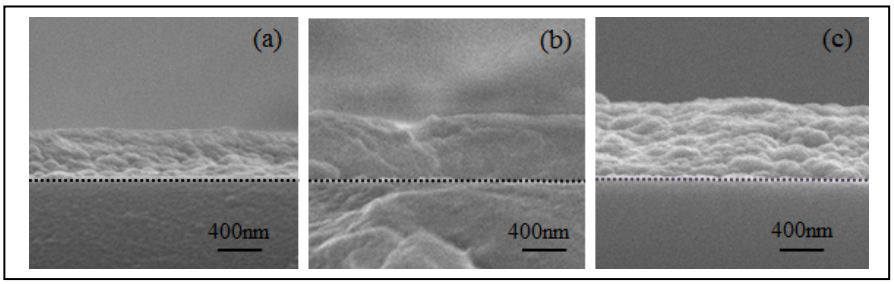

Figure 6 Cross-sectional SEM images of (a) [LDH(0.4 g/L)/SiO_2(25 nm)]$_6$, (b) [LDH(0.4 g/L)/SiO_2(25 nm)]$_8$ and (c) [LDH(0.4 g/L)/SiO_2(25 nm)]$_{10}$ coatings deposited on the glass substrates. The dotted lines are the boundaries between the coatings and the fractured glass substrates.

The AFM images of the [LDH(0.4 g/L)/SiO_2(25nm)]$_n$ (n = 6, 8, and 10) coatings (Figure 7) and the [LDH(0.4 g/L)/SiO_2(50nm)]$_n$ (n = 6, 8, and 10) coatings (Figure 8), reveal that they had textured surfaces. The textured surface traps light, leading to a broadband suppression in reflection [21]. Figures 7(d), 7(e), and 7(f) and Figures 8(d), 8(e), and 8(f) illustrate the AFM horizontal cross-section data.

The horizontal cross section data span the ranges of 30 nm to 55 nm, 40 nm to 90 nm, and 90 nm to 150 nm, which correspond to the [LDH/SiO_2(25 nm)]$_6$, [LDH/SiO_2(25 nm)]$_8$ and [LDH/SiO_2(25 nm)]$_{10}$ coatings, respectively. Similarly, the horizontal cross-section data span the ranges of 30 nm to 60 nm, 50 nm to 100 nm, 40 nm to 100 nm, which correspond to the [LDH/SiO_2(50 nm)]$_6$, [LDH/SiO_2(50 nm)]$_8$ and [LDH/SiO_2(50 nm)]$_{10}$ coatings, respectively. For SiO_2 nanoparticles with a diameter of 25 nm, the rms data were 25, 50, and 60, which correspond to the bilayers number of 6, 8, and 10, respectively. So the function may be $r = -1.875n^2 + 38.75n - 140$. For SiO_2 nanoparticles with a diameter of 50 nm, the rms data were 30, 50, and 60, which correspond to the bilayers number of 6, 8, and 10, respectively. So the function may be $r = -1.25n^2 + 27.5n - 90$. The function is an estimate due to the small data sample.

However, it can be seen in general that the surface roughness of the coatings increased in range with the increasing number of deposition cycles. The larger span ranges led to a more textured surface, which indicates that the surface roughness of the coatings increased with the increasing number of deposition cycles. Bravo, *et al*. pointed out that the level of transmittance tended to decrease as a result of the increasing roughness of the coatings and the increasing propensity to scatter light when more bi-layers were added to the multilayer that possesses the optimal anti-reflection property [23]. All of these findings mean that a moderately textured surface is needed to achieve the best

antireflection property by controlling the proper number of deposition cycles.

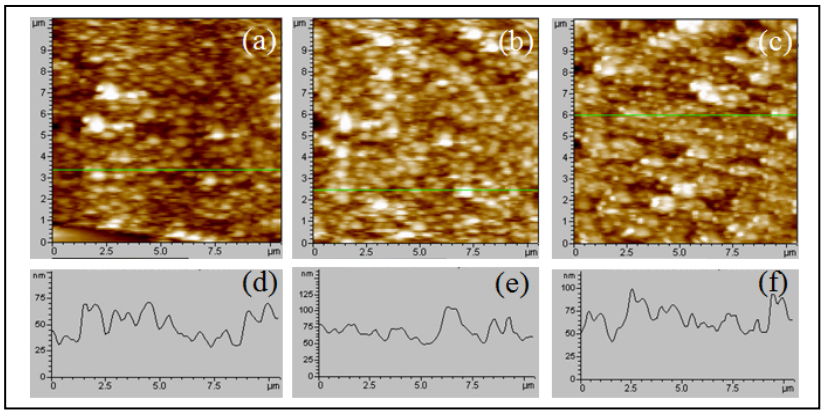

Figure 7 AFM images of (a) [LDH(0.4 g/L)/SiO_2(25 nm)]$_6$, (b) [LDH(0.4 g/L)/SiO_2(25 nm)]$_8$ and (c) [LDH(0.4 g/L)/SiO_2(25 nm)]$_{10}$ coatings. (d), (e) and (f) illustrate the AFM horizontal cross section data corresponding to (a), (b) and (c), respectively.

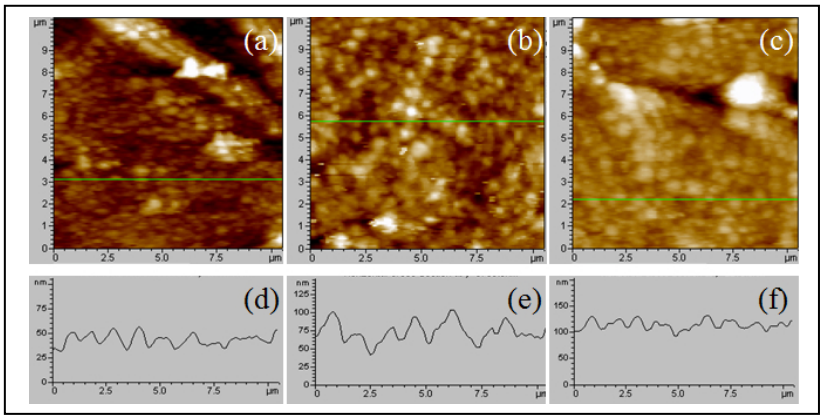

Figure 8 AFM images of (a) [LDH(0.4 g/L)/SiO_2(50 nm)]$_6$, (b) [LDH(0.4 g/L)/SiO_2(50 nm)]$_8$ and (c) [LDH(0.4 g/L)/SiO_2(50 nm)]$_{10}$ coatings. (d), (e) and (f) illustrate the AFM horizontal cross section data corresponding to (a), (b) and (c), respectively.

The anti-reflection properties of the LDH/SiO2 multilayer coatings were investigated using UV-vis transmission spectra. Figure 9(a) shows the UV-vis transmission spectra of glass substrates that were exclusively deposited with SiO2 nanoparticles. Figures 9(b), 9(c), and 9(d) shows the UV-vis transmission spectra of the glass substrates deposited with LDH/SiO2 multilayer coatings that differed in the number of dipping cycles n (n = 2, 4, 6, 8, and 10), LDH

content, and the diameters of silica nanoparticles. For comparison, the transmission spectrum of bare glass substrate is also depicted.

As can be seen from Figure 9, the bare glass substrate showed a transmittance of approximately 92% in the spectral range between 300 and 800 nm. Evidently, the coated slide glasses exhibited significantly enhanced transmittances in comparison with the bare glass substrate. As can be seen from Figure 9(a), transmission levels of 94% to 96% were achieved in the spectral range of 450 nm to 800 nm in the glass substrates deposited with single SiO_2 nanoparticles. As can be seen from Figure 9(b), among the $[LDH(0.4\ g/L)/SiO_2(25\ nm)]_n$ (n = 2, 4, 6, 8, and 10) coatings, the 8-bilayer coatings exhibited the best broadband antireflection properties.

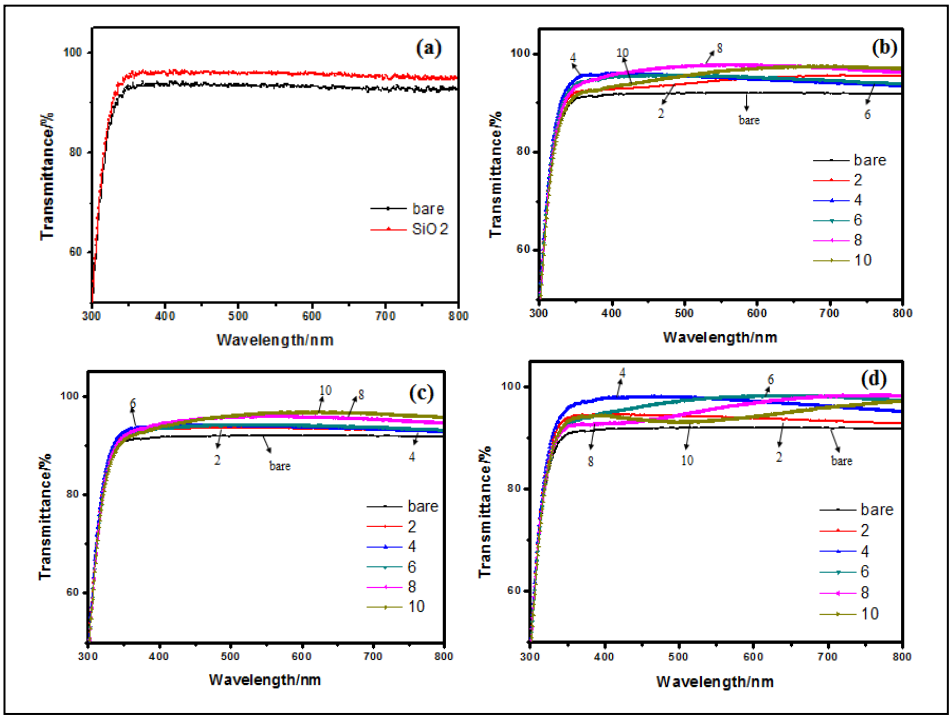

Figure 9 UV-vis transmission spectra of SiO_2 coatings and $(LDH/SiO_2)_n$ (n = 2, 4, 6, 8, and 10) coatings deposited on glass substrates. Multilayer coatings were on both sides of the glass substrates. (a) Coatings comprising of single SiO_2 nanoparticles, (b) $[LDH(0.4\ g/L)/SiO_2(25\ nm)]_n$ (n = 2, 4, 6, 8, and 10), (c) $[LDH(0.4\ g/L)/SiO_2(50\ nm)]_n$ (n = 2, 4, 6, 8, and 10), (d) $[LDH(0.8\ g/L)/SiO_2(25\ nm)]_n$ (n = 2, 4, 6, 8, 10).

In this 8-bilayer system, transmission levels of 96% to 98% and 98% to 96% were achieved in the spectral range of 420 to 550 and 550 nm to 800 nm,

respectively. Typically, a maximum transmittance of 98% was achieved at a wavelength of 550 nm, indicating that reflective loss was as low as about 2%. As can also be seen from Figures 9(b) and 9(c), the 10-bilayer coatings exhibited the best broadband anti-reflection properties among $[LDH(0.4\ g/L)/SiO2(50\ nm)]_n$ (n = 2, 4, 6, 8, and 10) and the 6-bilayer coatings exhibited the best broadband anti-reflection properties among [LDH(0.8 g/L)/SiO2(25 nm)]n (n = 2, 4, 6, 8, to 10). Typically, maximum transmittances of 97% and 98% were achieved at a wavelength of 625 and 700 nm, respectively. As discussed in the SEM and AFM analysis, the different packing patterns of the two oppositely charged nanomaterials and the moderately textured surface both determined the bilayer systems to be optimal, with high-performance broadband anti-reflection property.

Table 1 Transmittance of AR Coatings.

Transmittance /%	***n* = 2**	***n* = 4**	***n* = 6**	***n* = 8**	***n* = 10**
$[LDH(0.4\ g/L)/SiO_2(25\ nm)]_n$	95.5	96.0	95.5	98.0	97.5
$[LDH(0.4\ g/L)/SiO_2(50\ nm)]_n$	93.5	94.0	94.0	96.0	97.0
$[LDH(0.8\ g/L)/SiO_2(25\ nm)]_n$	94.5	98.0	98.0	98.0	97.0

The maximum transmittance of the AR coatings is shown in Table 1.

The results indicate that higher LDH concentrations cause a higher transmittance of the coatings in a broad spectral range. Although the transmittance of the coatings increases, the size of the nanoparticles decreases with the increase in LDH concentration.

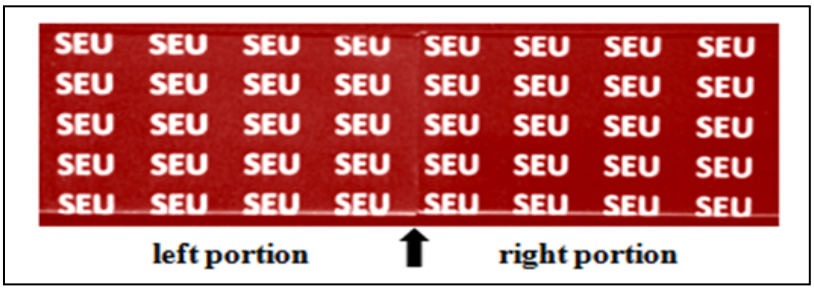

Figure 10 Photographic image exposed to sunlight. Left portion: slide glass without any coating. Right portion: slide glass with both sides covered with $[LDH(0.4\ g/L)/SiO2(25\ nm)]_8$ coatings.

Figure 10 presents the antireflection property of the [LDH(0.4 g/L)/ SiO_2(25 nm)]$_8$ coatings by visual observation. The words below the slide glass with the coatings (right portion) are clearer than those below the uncoated slide glass (left portion), demonstrating the enhancement in transparency and the decrease in reflectance that occurred at the coated slide glass.

4 Conclusion

In summary, our approach is based on a layer-by-layer self-assembly method using alternating layers of oppositely charged LDH nanosheets and silica nanoparticles within broadband antireflection coatings. The obtained [LDH(0.4 g/L)/SiO_2(25 nm)]$_8$, [LDH(0.4 g/L)/SiO_2(50 nm)]$_{10}$, [LDH(0.8 g/L)/ SiO_2(25 nm)]$_6$ coatings exhibited the best broadband anti-reflection property among the prepared LDH/SiO_2 multilayer coatings with different deposition cycles. In these optimal systems, transmission levels of 97% were achieved. Moreover, a maximum transmittance of 98% was achieved at a wavelength of 700 nm in the [LDH(0.8 g/L)/ SiO_2(25 nm)]$_6$ system. In short, both the proper packing arrangement, which means generating different packing patterns by distribution of dense packing LDH nanosheets and loose stacking silica nanoparticles as alternating layers and the moderately textured surface are beneficial to high-performance broadband antireflection properties by reducing wavelength dependence and enhancing reflectance suppression. The current approach may provide a new route to fabrication of broadband antireflection coatings with the advantages of easy availability of the materials and the simplicity of the method.

Acknowledgements

The authors acknowledge the financial support from the Natural Science Foundation of China (51077013) and Fund Project for Transformation of Scientific and Technological Achievements of Jiangsu Province of China (BA2011086); Scientific Innovation Research Foundation of College Graduate in Jiangsu Province (CXZZ13-0091, CXLX13-107). The authors are grateful to Prof. Huangxian Ju and Dr. Quanbo Wang at Nanjin University for their assistance with AFM characterization.

References

[1] Ho, P.K., Stephen, D., Friend, R.H. & Tessler, N., *All-polymer Optoelectronic Devices*, Science, **285**(5425), pp. 233-236, 1999.

[2] Yoldas, B.E., *Investigations of Porous Oxides as an Antireflective Coating for Glass Surfaces*, Applied Optics, **19**(9), pp. 1425-1429, 1980.

[3] Agáta R., Pavol H., Lucia K., Jana P., Tomáš Z. & Peter Mo., *Influence of Focusing Tube Wear on Vibrations and Surface Roughness*, Technical Gazette, **22**(2), pp. 271-278, 2015.
[4] Gu, G., Dang, H., Zhang, Z. & Wu, Z., *Fabrication and Characterization of Transparent Superhydrophobic Thin Films Based on Silica Nanoparticles*, Applied Physics A, **83**(1), pp. 131-132, 2006.
[5] Han, J., Dou, Y., Wei, M., Evans, D.G. & Duan, X., *Erasable Nanoporous Antireflection Coatings Based on the Reconstruction Effect of Layered Double Hydroxides*, Angewandte Chemie International Edition, **49**(12), pp. 2171-2174, 2010.
[6] Walheim, S., Schäffer, E., Mlynek, J. & Steiner, U., *Nanophase-Separated Polymer Films as High-Performance Antireflection Coatings*, Science, **283**(5401), pp. 520-522, 1999.
[7] Li, X., Xue, L. & Han, Y., *Broadband Antireflection of Block Copolymer/Homopolymer Blend Films with Gradient Refractive Index Structures*, Journal of Materials Chemistry, **21**(15), pp. 5817-5826, 2011.
[8] Zhang, L., Li, Y., Sun, J. & Shen, J., *Mechanically Stable Antireflection and Antifogging Coatings Fabricated by the Layer-by-Layer Deposition Process and Postcalcination*, Langmuir, **24**(19), pp. 10851-10857, 2008.
[9] Lim, H.S., Han, J.T., Kwak, D., Jin, M. & Cho, K., *Photoreversibly Switchable Superhydrophobic Surface with Erasable and Rewritable Pattern*, Journal of the American Chemical Society, **128**(45), pp. 14458-14459, 2006.
[10] Podsiadlo, P., Sui, L., Elkasabi, Y., Burgardt, P., Lee, J., Miryala, A. & Kotov, N.A., *Layer-by-Layer Assembled Films of Cellulose Nanowires with Antireflective Properties*, Langmuir, **23**(15), pp. 7901-7906, 2007.
[11] Zhang, L., Li, Y., Sun, J. & Shen J., *Layer-by-Layer Fabrication of Broad-Band Superhydrophobic Antireflection Coatings in Near-Infrared Region*, Journal of Colloid and Interface Science, **319**(1), pp. 302-308, 2008.
[12] Shimomura, H., Gemici, Z., Cohen, R.E. & Rubner, M.F., *Layer-by-Layer-Assembled High-Performance Broadband Antireflection Coatings*, ACS applied materials & interfaces, **2**(3), pp. 813-820, 2010.
[13] Zhang, L., Qiao, Z.A., Zheng, M., Huo, Q. & Sun, J., *Rapid and Substrate-Independent Layer-by-Layer Fabrication of Antireflection-and Antifogging-Integrated Coatings*, Journal of Materials Chemistry, **20**(29), pp. 6125-6130, 2010.
[14] Hibino, T. & Kobayashi, M., *Delamination of Layered Double Hydroxides in Water*, Journal of Materials Chemistry, **15**(6), pp. 653-656, 2005.
[15] Liu, Z., Ma, R., Osada, M., Iyi, N., Ebina, Y., Takada, K. & Sasaki, T., *Synthesis, Anion Exchange, and Delamination of Co-Al layered Double Hydroxide: Assembly of the Exfoliated Nanosheet/Polyanion Composite*

Films and Magneto-Optical Studies, Journal of the American Chemical Society, **128**(14): 4872-4880, 2006.

[16] Iyi, N., Matsumoto, T., Kaneko, Y. & Kitamura, K., *Deintercalation of Carbonate Ions from a Hydrotalcite-Like Compound: Enhanced Decarbonation Using Acid-Salt Mixed Solution*, Chemistry of materials, **16**(15), pp. 2926-2932, 2004.

[17] Li, L., Ma, R., Ebina, Y., Iyi, N. & Sasaki, T., *Positively Charged Nanosheets Derived via Total Delamination of Layered Double Hydroxides*, Chemistry of materials, **17**(17), pp. 4386-4391, 2005.

[18] Ma, R., Liu, Z., Li, L., Iyi, N. & Sasaki, T., *Exfoliating Layered Double Hydroxides in Formamide: a Method to Obtain Positively Charged Nanosheets*, Journal of Materials Chemistry, **16**(39), pp. 3809-3813, 2006.

[19] Han, J.B., Lu, J., Wei, M., Wang, Z.L. & Duan, X., *Heterogeneous Ultrathin Films Fabricated by Alternate Assembly of Exfoliated Layered Double Hydroxides and Polyanion*, Chemical Communications **41**, pp. 5188-5190, 2008.

[20] De, S., Jana, D., Medda, S.K. & De, G., *Wavelength Selective Antireflective Coatings on Plastics with Hydrophobic Surfaces*, Industrial & Engineering Chemistry Research, **52**(23), pp. 7737-7745, 2013.

[21] Lee, Y.J., Ruby, D.S., Peters, D.W., McKenzie, B.B. & Hsu, J. W., *ZnO Nanostructures as Efficient Antireflection Layers in Solar Cells*, Nano Letters, **8**(5), pp. 1501-1505, 2008.

[22] Xi, J.Q., Schubert, M.F., Kim, J.K., Schubert, E.F., Chen, M., Lin, S.Y. & Smart, J.A., *Optical Thin-Film Materials with Low Refractive Index for Broadband Elimination of Fresnel Reflection*, Nature Photonics, **1**(3): 176-179, 2007.

[23] Bravo, J., Zhai, L., Wu, Z., Cohen, R.E., Rubner, M.F., *Transparent Superhydrophobic Films based on Silica Nanoparticles*, Langmuir, **23**(13), pp. 7293-7298, 2007.